Pis'ma v ZhETF, vol. 100, iss. 2, pp. 141 – 150

ПО ИТОГАМ ПРОЕКТОВ
РОССИЙСКОГО ФОНДА ФУНДАМЕНТАЛЬНЫХ ИССЛЕДОВАНИЙ
Проекты РФФИ # 11-02-00112, # 12-02-31874

Status of the lepton $g-2$ and effects of hadronic corrections

A. E. Dorokhov[1)], *A. E. Radzhabov*[+], *A. S. Zhevlakov*[+]

Bogoliubov Laboratory of Theoretical Physics, Joint Institute for Nuclear Research, 141980 Dubna, Russia

Bogoliubov Institute of Theoretical Problems of Microworld, Lomonosov MSU, 119991 Moscow, Russia

[+]*Institute for System Dynamics and Control Theory SB RAS, 664033 Irkutsk, Russia*

Submitted 28 May 2014

The electron and muon anomalous magnetic moments (AMM) are measured in experiments and studied in the Standard Model (SM) with the highest precision accessible in particle physics. The comparison of the measured quantity with the SM prediction for the electron AMM provides the best determination of the fine structure constant. The muon AMM is more sensitive to the appearance of New Physics effects and, at present, there appears to be a three- to four-standard deviation between the SM and experiment. The lepton AMMs are pure relativistic quantum correction effects and therefore test the foundations of relativistic quantum field theory in general, and of quantum electrodynamics (QED) and SM in particular, with highest sensitivity. Special attention is paid to the studies of the hadronic contributions to the muon AMM which constitute the main source of theoretical uncertainties of the SM.

DOI: 10.7868/S0370274X14140124

1. Motivation. The anomalous magnetic moment (AMM) of charged leptons ($l = e, \mu, \tau$) is defined by

$$a_l = \frac{g_l - 2}{2}, \tag{1}$$

with the gyromagnetic ratio g_l of the lepton magnetic moment to its spin, in Bohr magneton units. For a free pointlike fermion one has $g = 2$ in accordance with the Dirac equation (Fig. 1a). However, deviations appear when taking into account the interactions leading to fermion substructure and thus to nonzero a_l (Figs. 1b–f).

During the first years of the lepton AMM studies the fundamental task was to test the foundations of quantum field theory in general and quantum electrodynamics (QED) in particular. At present, the measurements of the lepton AMM are one of the major low-energy tests of the standard model (SM) and play an important role in the search for new interactions beyond the SM.

The nonzero lepton AMMs are induced by radiative corrections due to the coupling of the lepton spin to virtual fields, which in the SM are induced by QED, weak and strong (hadronic) interactions[2)] (Fig. 1)

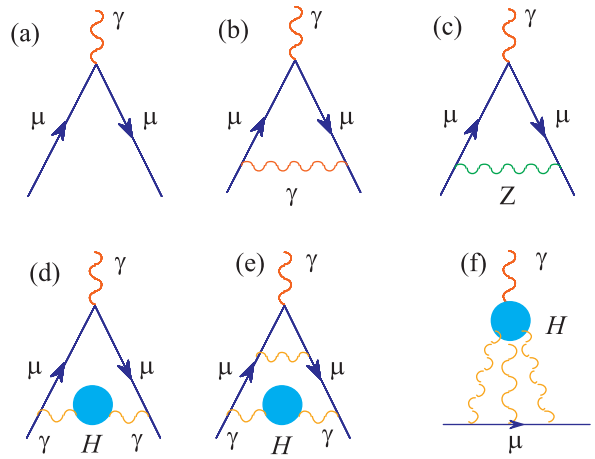

Fig. 1. Representative diagrams for the SM contributions to a_μ. Here, H is for the hadronic block

$$a^{\rm SM} = a^{\rm QED} + a^{\rm weak} + a^{\rm hadr}. \tag{2}$$

[1)]e-mail: dorokhov@theor.jinr.ru

[2)]For comprehensive reviews see [1, 2].

The electron and muon AMMs are among the most accurately measured quantities in elementary particle physics. Today, the electron AMM serves as the best quantity to determine the fine structure constant with the highest accuracy. At the same time, for a_μ, there is a deviation at the level of 3–4 σ of the SM prediction from the measured value. Even if this does not give a clear indication for the existence of New Physics, it allows us to provide stringent constraints on the parameters of hypothetical models.

The outline of this paper is as follows. In Section 2, we briefly report on the status of the electron AMM. In Section 3, the latest experimental and theoretical results on a_μ are presented. In Section 4, we review the most problematic theoretical input coming from the contribution due to the hadronic light-by-light (HLbL) scattering mechanism. Section 5 is devoted to some technical details of the calculations of the HLbL within the nonlocal chiral quark model (NχQM). Conclusions are presented in the last Section.

2. Electron AMM and fine structure constant. In 2008, the unique measurement by the Harvard group of Prof. G. Gabrielse, using a one-electron quantum cyclotron, obtained the electron AMM with unprecedented accuracy [3]

$$a_e^{\rm Harvard} = 1\ 159\ 652\ 180.73\ (0.28)\cdot 10^{-12} \quad [0.24\ \text{ppb}]. \tag{3}$$

This result leads to the determination of the fine structure constant α with the extraordinary precision [4, 5]

$$\alpha^{-1} = 137.035\ 999\ 1727\ (341) \quad [0.25\ \text{ppb}]. \tag{4}$$

The latter became possible after the complete QED contribution to the electron AMM up to tenth order in the coupling constant were achieved numerically by the Prof. T. Kinoshita group [4] (for recent review see [5])[3] by the Prof. T. Kinoshita group [4] (for recent review see [5]). Note, that the uncertainty in (4) is dominated by the uncertainty in the measurement of $a_e^{\rm Harvard}$.

The value in (4) has the highest precision of any value of α currently available [7]. Thus, a new measurement [8] of the ratio $h/m_{\rm Rb}$ between the Planck constant and the mass of ^{87}Rb atom studied by atom recoil leads to a value of the fine structure constant [7] $\alpha^{-1}\,(\text{Rb}) = 137.035\ 999\ 049\ (90)$ [0.66 ppb]. By using this α one gets for the electron AMM

$$a_e^{\rm SM}\,(\text{Rb}) = 1\ 159\ 652\ 181.78\ (0.77)\cdot 10^{-12} \quad [0.66\ \text{ppb}], \tag{5}$$

that is in agreement with the measurement (3).

3. Muon AMM: experiment vs theory. In 2006, there were published the results on a_μ measurements by the E821 Collaboration at Brookhaven National Laboratory (BNL) [9]. The combined result, based on nearly equal samples of positive and negative muons, is[4]

$$a_\mu^{\rm BNL} = 116\ 592\ 08.0\ (6.3)\cdot 10^{-10} \quad [0.54\ \text{ppm}]. \tag{6}$$

This exiting result is still limited by the statistical errors and proposals to measure a_μ with a fourthfold improvement in accuracy have been proposed at Fermilab (USA) [10] and J-PARC (Japan) [11]. A future experiments plan to reduce the present experimental error to a precision of 0.14 ppm.

In SM the dominant contribution to the lepton AMM comes from QED (Fig. 1b). The complete tenth-order QED contribution to a_μ was reported in [12]

$$a_\mu^{\rm QED} = 11\ 658\ 471.8951\ (0.0080)\cdot 10^{-10}. \tag{7}$$

The accuracy of these calculations is enough for any planed experiments in new future.

In general, the weak contributions (Fig. 1c) are small due to suppressing factor $\alpha/\pi\cdot m_\mu^2/M_w^2 \sim 10^{-9}$, where M_w is a typical mass of heavy $W^\pm, Z$, and H bosons. The one- and two-loop evaluations indicate that they are known with a sufficiently high accuracy [13, 14]

$$a_\mu^{\rm weak} = 15.36\ \ (0.10)\cdot 10^{-10}, \tag{8}$$

where the remaining theory error comes from the unknown three-loop contributions and dominantly from light hadronic uncertainties in the second-order electroweak diagrams with quark triangle loops. The most important feature of these new estimates, that significantly increase the theoretical precision, is to use the LHC result on the Higgs-boson mass measured by ATLAS [15, 16] and CMS [17, 18] Collaborations.

Strong (hadronic) interaction produces relatively small contributions to a_μ, however they are known with an accuracy comparable to the experimental uncertainty in (6). In leading in α orders, these contributions can be separated into three terms

$$a_\mu^{\rm hadr} = a_\mu^{\rm HVP} + a_\mu^{\rm ho} + a_\mu^{\rm HLbL}. \tag{9}$$

In (9), $a_\mu^{\rm HVP}$ is the leading in α contribution due to the hadron vacuum polarization (HVP) effect in the internal photon propagator of the one-loop diagram (Fig. 1d),

[3] The famous analytical result at six order is known due to work by Laporta and Remiddi [6].

[4] Later on this value was corrected [7] for a small shift in the ratio of the magnetic moments of the muon and the proton as $a_\mu^{\rm BNL,corr} = 116\ 592\ 09.1\ (6.3)\cdot 10^{-10}$.

$a_\mu^{\rm ho}$ is the next-to-leading order contribution related to iteration of HVP (Fig. 1e). The last term is not reduced to HVP iteration and it is due to the hadronic light-by-light (HLbL) scattering mechanism (Fig. 1f).

Hadronic contributions in (9) are determined by effects dominated by long distance dynamics, the region where the methods of perturbation theory of Quantum Chromodynamics (QCD) do not applicable and one must use less reliable nonperturbative approaches. However, in case of HVP, using analyticity and unitarity (the optical theorem) $a_\mu^{\rm HVP}$ can be expressed as the spectral representation integral [19]

$$a_\mu^{\rm HVP} = \frac{\alpha}{\pi}\int_{4m_\pi^2}^{\infty}\frac{dt}{t}K(t)\rho_{\rm V}^{\rm (H)}(t)\,, \qquad (10)$$

which is a convolution of the hadronic spectral function

$$\rho_V^{\rm (H)}(t) = \frac{1}{\pi}\,{\rm Im}\,\Pi^{\rm (H)}(t) \qquad (11)$$

with the known from QED kinematical factor

$$K(t) = \int_0^1 dx\frac{x^2(1-x)}{x^2+(1-x)t/m_\mu^2}, \qquad (12)$$

where m_μ is the muon mass. The QED factor is sharply peaked at low invariant masses t and decreases monotonically with increasing t. Thus, the integral defining $a_\mu^{\rm HVP}$ is sensitive to the details of the spectral function $\rho_V^{\rm (H)}(t)$ at low t. At present there are no direct theoretical tools that allow one to calculate the spectral function at low t with required accuracy. Fortunately, $\rho_V^{\rm (H)}(t)$ is related to the total $e^+e^-\to\gamma^*\to$ hadrons cross-section $\sigma(t)$ at center-of-mass energy squared t by

$$\sigma^{e^+e^-\to{\rm hadrons}}(t) = \frac{4\pi\alpha}{t}\rho_V^{\rm (H)}(t)\,, \qquad (13)$$

and this fact is used to get quite accurate estimate of $a_\mu^{\rm HVP}$. The most precise recent phenomenological evaluations of $a_\mu^{\rm HVP}$, using recent $e^+e^-\to$ hadrons data, provide the results

$$a_\mu^{{\rm HVP},e^+e^-} = \begin{cases} 692.3\ \ (4.2)\cdot 10^{-10} & [20], \\ 694.91\ \ (4.27)\cdot 10^{-10} & [21]. \end{cases} \qquad (14)$$

In addition, data on inclusive decays of the τ-lepton into hadrons are used to replace the e^+e^- data in certain energy regions. This is possible, since the vector current conservation law relates the $I=1$ part of the electromagnetic spectral function to the charged current vector spectral function measured in $\tau\to\nu$ +non-strange hadrons (see, i.e., [22]). All these allow one to reach a substantial improvement in the accuracy of the contribution from the HVP during the last decade.

Similar, the dispersion relation approach and the same phenomenological input lead to the estimate of the next-to-leading hadronic contribution (Fig. 1e) [21]

$$a_\mu^{\rm ho} = -9.84\ \ (0.08)\cdot 10^{-10}. \qquad (15)$$

Thus, the HVP and next-to-leading order contribution related to HVP are known with an accuracy better than 1 per cent.

In near future it is expected that new and precise measurements from CMD3 and SND at VEPP-2000 in Novosibirsk, BES III in Beijing and KLOE-2 at DAFNE in Frascati allow to significantly increase accuracy of predictions for $a_\mu^{\rm HVP}$ and $a_\mu^{\rm ho}$ and resolve some inconsistency problems between different set of data.

Combining all SM contributions one gets

$$a_\mu^{\rm SM} = 116\ 591\ 80.2\ (0.1)_{\rm EW}(0.08)_{\rm ho}(4.2)_{\rm HVP}(2.6)_{\rm HLbL} \times 10^{-10}, \qquad (16)$$

where we take for the leading order evaluations given in (14a) and the guessed value for the hadronic light-by-light contribution from [23]

$$a_\mu^{\rm HLbL}({\rm Guess}) = 10.5\ \ (2.6)\cdot 10^{-10}. \qquad (17)$$

The latter contribution will be discussed below with details. The resulting difference between the experimental result (6) and the full SM prediction is

$$a_\mu^{\rm BNL} - a_\mu^{\rm SM} = 28.7\ \ (8.0)\cdot 10^{-10}, \qquad (18)$$

which signals on 3.6 σ discrepancy between theory and experiment. The SM theoretical error is dominated by the hadronic contributions. In that respect theoretical predictions of HVP and HLbL contributions to a_μ should be at the same level or better than a precision of planed experiments.

4. Status of the hadronic light-by-light scattering contribution to a_μ. The next-to-leading order corrections are suppressed by the absolute value by extra degree of α. However, one kind of these contributions corresponding to the HLbL (Fig. 1f), is of amount ranging from 0.5 to 1.5 ppm and known with accuracy of order 50 %[5)]. It gives an error comparable in magnitude with the uncertainty induced by HVP (14). The problem is that the HLbL scattering contribution can not be calculated from first principles or (unlike to HVP) directly extracted from phenomenological considerations.

[5)] In QED, the LbL contributions due to virtual charged fermions at six order level was analytically elaborated in [24, 25]. At the same level of accuracy the result for the virtual scalars was obtained in [25].

Table 1

Model estimates of the HLbL contribution to a_μ from various sources obtained in different works. All numbers are given in 10^{-10}. The errors do not include the systematic error of the models

Model	π^0	PS (π^0, η, η')	S (σ, f_0, a_0)	AV	Quark loop	$\pi, K-$ loops	Total
VMD (Hayakawa [27])	5.74(0.36)	8.27(0.64)		0.17(0.17)	0.97(1.11)	−0.45(0.81)	8.96(1.54)
ENJL (Bijnens [28])	5.94(0.2)	8.5(1.3)	−0.68(0.2)	0.25(0.1)	2.1(0.3)	−1.9(1.3)	8.3(3.2)
LMD+V (Knecht [29])	5.8(1.0)	8.3(1.2)					8.3(1.2)
Q-box (Pivovarov [35])					14.3		14.3
LENJL (Bartos [34])	8.18(1.65)	9.55(1.7)	1.23(0.24)				10.77(1.68)
(LMD+V)′ (Melnikov [30])	7.65(1.0)	11.4(1.0)		2.2(0.5)		0(10)	13.6(2.5)
NχQM (Dorokhov [39, 40, 45])	5.01(0.37)	5.85(0.87)	0.34(0.48)		11.0(0.9)		16.8(1.25)
oLMDV (Nyffeler [31])	7.2(1.2)	9.9(1.6)	−0.7(0.2)	2.2(0.5)	2.1(0.3)	−1.9(1.3)	11.6(4.0)
DS (Goecke [41])	5.75(0.69)	8.07(1.2)			10.7(0.2)		18.8(0.4)
CχQM (Greynat [38])	6.8(0.3)	6.8(0.3)			8.2(0.6)		15.0(0.3)

Instead, it has to be evaluated using various QCD inspired hadronic models that correctly reproduce low- and high-energy properties of strong interaction. Nevertheless, as will be discussed below, it is important for the model calculations that phenomenological information and well established theoretical principles should significantly reduce the number of model assumptions and the allowable space of model parameters.

In general, the HLbL scattering amplitude is a complicated object for calculations. It is a sum of different diagrams including the dynamical quark loop, the meson exchanges, the meson loops and the iterations of these processes. Fortunately, already in the first papers devoted to the calculation of the HLbL contributions [26–28], it has been recognized that these numerous terms show a hierarchy. This is related to existence of two small parameters: the inverse number of colors $1/N_c$ and the ratio of the characteristic internal momentum to the chiral symmetry parameter $m_\mu/(4\pi f_\pi) \sim 0.1$. The former suppresses the multiloop contributions, so that the leading contribution is due to the quark loop diagram and the two-loop diagrams with mesons in the intermediate state. In latter case, the contribution of the diagram with intermediate pion is enhanced by small pion mass in the meson propagator.

Different approaches to the calculation of the contributions from the HLbL scattering process to a_μ were used. These approaches can be separated in several groups. The first one consists of various extended versions of the vector meson dominance model (VMD) supplemented by ideas of the chiral effective theory, such as the hidden local symmetry model (HLS) [27], the lowest meson dominance (LMD) [29–31], the resonance chiral theory (RχT) [32, 33]. The second group is based on consideration the effective models of QCD that use the dynamical quarks as effective degrees of freedom. The latter include different versions of the (extended) Nambu–Jona–Lasinio model (E)NJL [28, 34], the Constituent Quark Models with local interaction (CQM) [35–38], the models based on nonperturbative quark-gluon dynamics, like the non-local chiral quark model (NχQM) [39, 40], the Dyson–Schwinger model [41] (DS), or the holographic models (HM) [42, 43]. The lattice calculations of HLbL are still at an exploratory stage [44].

The results of model calculations are given in Tables 1 and 2. Table 1 contains the model results where few sources of contributions can be identif[6)]. In Table 2 there are the model results where only contribution of the light pseudoscalar mesons is calculated.

Table 2

The HLbL contribution to a_μ from the mesonic exchanges in the neutral pseudoscalar channel obtained in different works. All numbers are given in 10^{-10}

Model	π^0	PS
Holography (Hong [42])	6.9	10.7
Holography (Cappiello [43])	6.54(0.25)	
RχT (Kampf [32])	6.58(0.12)	
RχT (Roig [33])	6.66(0.21)	10.47(0.54)

To reduce the model dependence of various approaches, different constraints on their parameter space are employed. One kind of important constraints on the models follows from the phenomenology of the two-

[6)] The NχQM results for the pion and pseudoscalar mesons exchanges are taken from [39]. The scalar mesons contribution is corrected value of (from 0.39(0.04) [40] to 0.34(0.48) [45]). The dynamical quark-loop contribution and the total result are taken from [45].

photon widths of the pseudoscalar mesons $\Gamma(PS \to \gamma\gamma)$ and their transition form factors $\mathrm{F}_{PS\gamma\gamma^*}\left(-M_{PS}^2; 0, q^2\right)$ first emphasized in [27]. Another set of constraints follows from the large momentum asymptotics for the meson transition form factors [27–29] and for the total light-by-light scattering amplitude considered in [30, 39, 40], obtained using perturbative QCD and reproduced within the NχQM.

In addition, the model amplitudes have to be consistent with the 4-momentum conservation law. In practice, it means that the off-shell effects for intermediate mesons should be taken into account [1, 39, 40]. For illustration of this effect see Fig. 2 from [39].

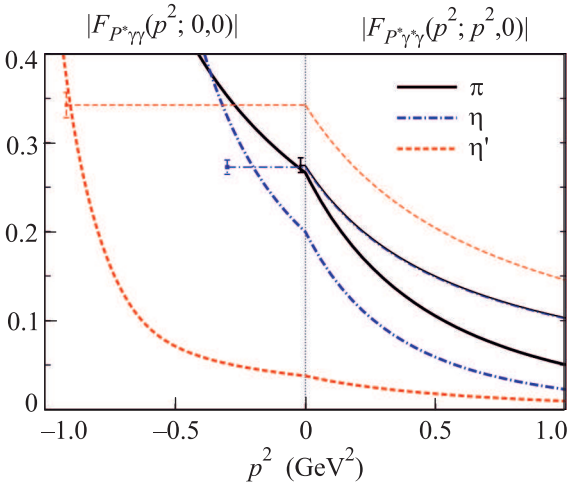

Fig. 2. Plots of the π^0, η, and η' vertices $F_{P^*\gamma\gamma}(p^2; 0, 0)$ in the timelike region and $F_{P^*\gamma^*\gamma}(p^2; p^2, 0)$ in the spacelike region in NχQM model (thick lines) and VMD model (thin lines). The points with error bars correspond to the physical points of the meson decays into two photons. The VMD curves for π^0 and η are almost indistinguishable

Finally, the model calculations should be tested by reproducing the dispersion analysis result for the HVP contribution to a_μ as it was done in [26, 46, 35, 47, 38] and the known (semi)analytical results on the fermion-loop contributions to the lepton AMM as it was done in [35, 37, 40, 38]. In this respect note, that in [48] the CQM expression of [37] for the 4-loop HLbL contribution to the a_μ was used for analytical evaluation of the first term of eighth-order (m_μ/m_τ) contribution to a_μ and (m_e/m_τ) and (m_e/m_μ) contributions to a_e. The analytical results turned out to be in good agreement with the numerical results of calculations of these 8-th order massive corrections, re-evaluated in the process of obtaining 10-th order corrections to a_e in [4] and complete 10-th order corrections to a_μ [12]. In [48] the statement was made, that the comparison of the results obtained in [48] with the numerical calculations of the 8-order massive dependent corrections indicate that the numerical results are also sensitive to higher order power-suppressed massive-dependent corrections. This statement was confirmed by direct analytical calculations, performed recently in [49]. These QED calculations of [48] and [49] and the comparison with the results of numerical 8-th order QED calculations of [4] demonstrate, that the CQM calculations of 8-th order light-by-light contributions to a_μ of [37] are correct.

In next part we discuss the HLbL contribution as it is calculated within the NχQM and show that, within this framework, it might be possible realistically to determine this value to a sufficiently safe accuracy. We want to discuss how well this model (see, e.g., [50]) does in calculating a_μ^{HLbL}. Below, within the NχQM, we discuss with some details theoretical status of HLbL contributions to a_μ due to the exchange by light mesons and the dynamical quark loop.

5. HLbL contribution to the muon AMM within nonlocal chiral quark model. *5.1. NχQM dynamics.* The NχQM is an effective QCD inspired model that has a numerous applications for description of low energy hadronic dynamics [50]. We mention only those applications that are related to the problem of hadronic contributions to a_μ. The two-point VV correlator has been calculated in [51] and used for calculations of a_μ^{HVP} [47]. The three-point VAV correlator has been studied in [52] and used for calculations of the hadronic photon-Z-boson vertex contribution to a_μ [53]. The HLbL corrections due to light meson exchanges and specific HVP corrections, where the virtual photon splits into π^0 (σ) and γ, was elaborated in [39, 40]. Note that the NχQM approach in many ways similar to ENJL [28] and DS [41] models with, of course, subtle differences between all of them.

The Lagrangian of the $SU(3) \times SU(3)$ chiral quark model has the form

$$\mathcal{L} = \bar{q}(x)(i\hat{\partial} - m_c)q(x) + \\ + \frac{G}{2}[J_S^a(x)J_S^a(x) + J_{PS}^a(x)J_{PS}^a(x)] - \\ - \frac{H}{4}T_{abc}[J_S^a(x)J_S^b(x)J_S^c(x) - 3J_S^a(x)J_{PS}^b(x)J_{PS}^c(x)], \quad (19)$$

where $q(x)$ are the quark fields, m_c $(m_u = m_d \neq m_s)$ is the diagonal matrix of the quark current masses, G and H are the four- and six-quark coupling constants. Second line in the Lagrangian represents the Kobayashi–Maskawa–t'Hooft determinant vertex with the structural constant

$$T_{abc} = \frac{1}{6}\epsilon_{ijk}\epsilon_{mnl}(\lambda_a)_{im}(\lambda_b)_{jn}(\lambda_c)_{kl},$$

where λ_a are the Gell-Mann matrices for $a = 1, \ldots, 8$ and $\lambda_0 = \sqrt{2/3}I$.

The nonlocal structure of the model is introduced via the nonlocal quark currents

$$J^a_M(x) = \int d^4x_1 d^4x_2\, f(x_1) f(x_2)\, \bar{q}(x-x_1)\, \Gamma^a_M q(x+x_2), \tag{20}$$

where $M = S$ for the scalar and $M = PS$ for the pseudoscalar channels, $\Gamma^a_S = \lambda^a$, $\Gamma^a_{PS} = i\gamma^5\lambda^a$, and $f(x)$ is a form factor with the nonlocality parameter Λ reflecting the nonlocal properties of the QCD vacuum.

The model (19) can be bosonized using the stationary phase approximation which leads to the system of gap equations for the dynamical quark masses $m_{d,i}$

$$m_{d,i} + GS_i + \frac{H}{2} S_j S_k = 0, \tag{21}$$

with $i = u, d, s$ and $j, k \neq i$, and S_i is the quark loop integral

$$S_i = -8N_c \int \frac{d^4_E k}{(2\pi)^4} \frac{f^2(k^2) m_i(k^2)}{D_i(k^2)},$$

where $m_i(k^2) = m_{c,i} + m_{d,i} f^2(k^2)$, $D_i(k^2) = k^2 + m_i^2(k^2)$ is the dynamical quark propagator obtained by solving the DS equation, $f(k^2)$ is the nonlocal form factor in the momentum representation.

The quark-meson vertex functions and the meson masses can be found from the Bethe–Salpeter equation Fig. 3. For the separable interaction (19) the quark-

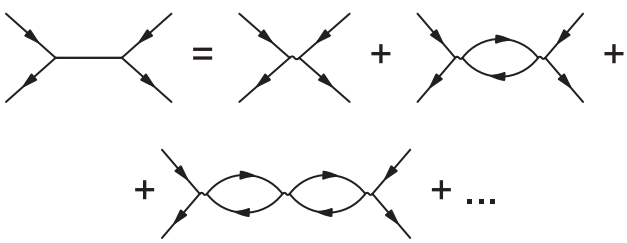

Fig. 3. The Bethe-Salpeter equation for meson propagators. The 4-quark crosses are for the interaction term (19)

antiquark scattering matrix in each (PS or S) channels becomes

$$\mathbf{T} = \hat{\mathbf{T}}(p^2)\delta^4\left[p_1 + p_2 - (p_3 + p_4)\right] \prod_{i=1}^{4} f(p_i^2),$$

$$\hat{\mathbf{T}}(p^2) = i\gamma_5\lambda_k \left(\frac{1}{-\mathbf{G}^{-1} + \mathbf{\Pi}(p^2)}\right)_{kl} i\gamma_5\lambda_l, \tag{22}$$

where p_i are the momenta of external quark lines, $\mathbf{G}$ and $\mathbf{\Pi}(p^2)$ are the corresponding matrices of the four-quark coupling constants and the polarization operators of mesons ($p = p_1 + p_2 = p_3 + p_4$). The meson masses can be found from the zeros of determinant $\det[\mathbf{G}^{-1} - \mathbf{\Pi}(-M^2)] = 0$. The $\hat{\mathbf{T}}$-matrix for the system of mesons in each neutral channel can be expressed as

$$\hat{\mathbf{T}}_{\rm ch}(P^2) = \sum_{M_{\rm ch}} \frac{\overline{V}_{M_{\rm ch}}(P^2) \otimes V_{M_{\rm ch}}(P^2)}{-(P^2 + \mathrm{M}^2_{M_{\rm ch}})}, \tag{23}$$

where M_M are the meson masses, $V_M(P^2)$ are the vertex functions $\left(\overline{V}_M(p^2) = \gamma^0 V^\dagger_M(P^2)\gamma^0\right)$. The sum in (23) is over full set of light mesons: ($M_{PS} = \pi^0, \eta, \eta'$) in the pseudoscalar channel and ($M_S = a_0(980), f_0(980), \sigma$) in the scalar one.

5.2. External photon fields. The gauge-invariant interaction with an external photon field V^a_μ can be introduced through the Schwinger phase factor

$$q(y) \to Q(x,y) = \mathcal{P}\exp\left[i\int_x^y dz^\mu V^a_\mu(z)\, T^a\right] q(y). \tag{24}$$

Then, apart from the kinetic term, the additional terms in the nonlocal interaction are generated via

$$J^a_M(x) \to J^a_M(x) = \int d^4x_1 d^4x_2\, f(x_1) f(x_2) \times \\ \times\, \overline{Q}(x - x_1, x)\, \Gamma^a_M Q(x, x + x_2), \tag{25}$$

which induces the quark-antiquark–n-photon vertices. Additionally, there appear the meson–quark-antiquark–n-photon vertices. The following equations are used for obtaining the nonlocal vertices [54]

$$\frac{\partial}{\partial y^\mu}\int_x^y dz^\nu V_\nu(z) = V_\mu(y),$$
$$\delta^{(4)}(x-y)\int_x^y dz^\nu V_\nu(z) = 0. \tag{26}$$

As an example, the quark-antiquark vertices with one-photon (Fig. 4a) and two-photon (Fig. 4b) inser-

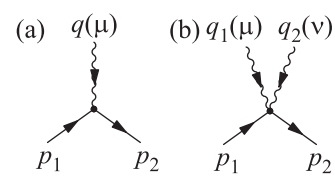

Fig. 4. The quark-photon vertex $\Gamma^{(1)}_\mu(q)$, Eq. (27) (a), and the quark-2-photon vertex $\Gamma^{(2)}_{\mu\nu}(q_1, q_2)$, Eq. (29) (b)

tions are

$$\Gamma^{(1)}_\mu = \gamma_\mu + \Delta\Gamma^{(1)}_\mu(q_1), \tag{27}$$

$$\Delta\Gamma^{(1)}_\mu(q_1) = -(p_1 + k_1)_\mu\, m^{(1)}(p_1, k_1), \tag{28}$$

$$\Gamma^{(2)}_{\mu\nu}(q_1, q_2) = 2g_{\mu\nu} m^{(1)}(p_1, k_{12}) + \\ + (p_1 + k_1)_\mu (k_1 + k_{12})_\nu\, m^{(2)}(p_1, k_1, k_{12}) + \\ + (p_1 + k_2)_\nu (k_2 + k_{12})_\mu\, m^{(2)}(p_1, k_2, k_{12}), \tag{29}$$

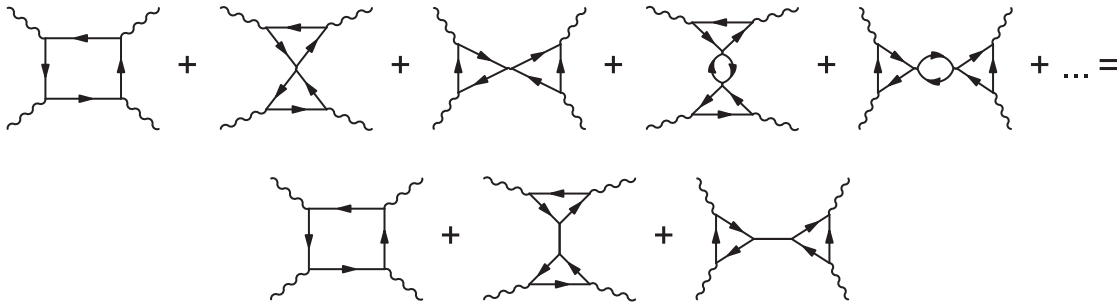

Fig. 5. A schematic illustration for the diagrams contributing to the four-rank polarization tensor to the leading in $1/N_c$ order. The nonlocal multi-photon vertices are not shown for simplicity, see Fig. 9

where the finite-difference derivatives are introduced

$$f^{(1)}(a,b)=\frac{f(a+b)-f(b)}{(a+b)^2-b^2}, \tag{30}$$

$$f^{(2)}(a,b,c)=\frac{f^{(1)}(a,b)-f^{(2)}(a,c)}{(a+b)^2-(a+c)^2},\ldots \tag{31}$$

In (27)–(29), p_1 is the momentum of incoming quark, q_i are the momenta of incoming photons, and $k_1=k+q_1$, $k_{ij\ldots k}=p_1+q_i+q_j+\ldots+q_k$. The vertex Γ_μ satisfies the Ward–Takahashi identity for dynamical quarks

$$q_1\Gamma^{(1)}_\mu=S^{-1}(p_1+q_1)-S^{-1}(p_1), \tag{32}$$

with

$$S^{-1}(p)=\hat{p}-m(p), \tag{33}$$

and for the multi-photon nonlocal vertices one has

$$q_1^\mu\Delta\Gamma^{(1)}_\mu(q_1)=m(p_1)-m(k_1), \tag{34}$$

$$q_1^\mu q_2^\nu\Gamma^{(2)}_{\mu\nu}(q_1,q_2)=m(p_1)+m(k_{12})-m(k_1)-m(k_2).$$

5.3. Hadronic light-by-light contribution to a_μ within $N\chi QM$. The basic element for the calculations of $a_\mu^{\rm HLbL}$ is the fourth-rank light quark hadronic vacuum polarization tensor

$$\Pi_{\mu\nu\lambda\rho}(q_1,q_2,q_3)=\int d^4x_1\int d^4x_2\int d^4x_3\times \tag{35}$$

$$\times e^{i(q_1x_1+q_2x_2+q_3x_3)}\langle 0|T(j_\mu(x_1)j_\nu(x_2)j_\lambda(x_3)j_\rho(0))|0\rangle,$$

where $j_\mu(x)$ are the light quark electromagnetic currents and $|0\rangle$ is the QCD vacuum state. The muon AMM can be extracted by using the projection [55]

$$a_\mu^{\rm HLbL}=\frac{1}{48m_\mu}{\rm Tr}\left[(\hat{p}+m_\mu)[\gamma^\rho,\gamma^\sigma](\hat{p}+m_\mu)\Pi_{\rho\sigma}(p,p)\right],$$

where

$$\Pi_{\rho\sigma}(p',p)=$$
$$=-ie^6\int\frac{d^4q_1}{(2\pi)^4}\int\frac{d^4q_2}{(2\pi)^4}\frac{1}{q_1^2q_2^2(q_1+q_2-k)^2}\times$$
$$\times\gamma^\mu\frac{\hat{p}'-\hat{q}_1+m_\mu}{(p'-q_1)^2-m_\mu^2}\gamma^\nu\frac{\hat{p}-\hat{q}_1-\hat{q}_2+m_\mu}{(p-q_1-q_2)^2-m_\mu^2}\gamma^\lambda\times$$
$$\times\frac{\partial}{\partial k^\rho}\Pi_{\mu\nu\lambda\sigma}(q_1,q_2,k-q_1-q_2), \tag{36}$$

with m_μ is the muon mass, $k_\mu=(p'-p)_\mu$ and it is necessary to make the limit $k_\mu\to 0$.

In the NχQM, the tensor $\Pi_{\mu\nu\lambda\rho}$ is represented in the leading in $1/N_c$ order by the chain of diagrams schematically depicted in Fig. 5. In the higher order contributions, the $1/N_c$ suppression factor coming from the four-quark interaction (19) is compensated by the N_c factor from the color trace of the quark loop. This infinite series of quark loop diagrams is summed up leading to the quark box and the diagrams with light meson exchanges. The double chain summation generates the meson loop contributions which are, however, suppressed by $1/N_c$ factor.

The HLbL contribution due to exchange of pseudoscalar (PS) and scalar (S) mesons (Fig. 6) was elaborated in [39]. The vertices containing the virtual (off-shell) meson M with momentum p and two virtual photons with momenta $q_{1,2}$ and the polarization vectors $\epsilon_{1,2}$ can be written as [34]

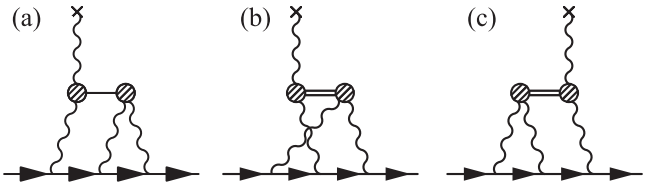

Fig. 6. The HLbL contribution from the intermediate light meson exchanges

$$\mathcal{A}\left(\gamma^*_{(q_1,\epsilon_1)}\gamma^*_{(q_2,\epsilon_2)}\to M^*_{(p)}\right)=e^2\epsilon_1^\mu\epsilon_2^\nu\Delta^{\mu\nu}_{M^*\gamma^*\gamma^*}(p;q_1,q_2), \tag{37}$$

where for the pseudoscalar mesons

$$\Delta^{\mu\nu}_{PS^*\gamma^*\gamma^*}(p;q_1,q_2) = -i\varepsilon_{\mu\nu\rho\sigma}q_1^\rho q_2^\sigma \mathrm{F}_{PS^*\gamma^*\gamma^*}\left(p^2;q_1^2,q_2^2\right), \tag{38}$$

and for the scalar mesons

$$\Delta^{\mu\nu}_{S^*\gamma^*\gamma^*}(p;q_1,q_2)=A_{S^*\gamma^*\gamma^*}\left(p^2;q_1^2,q_2^2\right)T_A^{\mu\nu}(q_1,q_2)+ \\ + B_{S^*\gamma^*\gamma^*}(p^2;q_1^2,q_2^2)T_B^{\mu\nu}(q_1,q_2), \tag{39}$$

and the Lorentz structures are

$$T_A^{\mu\nu}(q_1,q_2) = g^{\mu\nu}(q_1q_2) - q_1^\nu q_2^\mu, \tag{40}$$

$$T_{B'}^{\mu\nu}(q_1,q_2) = \left[q_1^2q_2^\mu - (q_1q_2)q_1^\mu\right]\left[q_2^2q_1^\nu - (q_1q_2)q_2^\nu\right], \tag{41}$$

and $p = q_1+q_2$. The subject of model calculations [39] is to get the (PS/S)*V*V* vertex functions $\mathrm{F}_{PS}, A_S, B_S$.

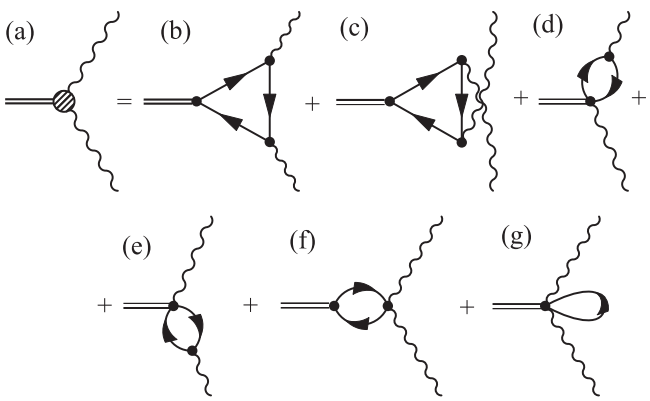

Fig. 7. The diagrams for the photon-meson vertices $\mathrm{F}_{PS^*\gamma^*\gamma^*}, A_{S^*\gamma^*\gamma^*}, B_{S^*\gamma^*\gamma^*}$. In the case of pseudoscalar mesons, the diagrams (d-g) give zero contributions due to chirality considerations

The expression for a_μ^{HLbL} from the light meson exchanges can be written in a three-dimensional integral representation as follows

$$a_\mu^{\mathrm{HLbL,MesExch}} = -\frac{2\alpha^3}{3\pi^2}\int\limits_0^\infty dQ_1^2\int\limits_0^\infty dQ_2^2\int\limits_{-1}^1 dt\sqrt{1-t^2}\times \\ \times\frac{1}{Q_3^2}\sum_M\left[2\frac{\mathcal{N}_1^M(Q_1^2,Q_2^2,Q_3^2)}{Q_2^2+M_M^2}+\frac{\mathcal{N}_2^M(Q_1^2,Q_3^2,Q_2^2)}{(Q_3^2+M_M^2)}\right], \\ \mathcal{N}_{\mathbf{1,2}}^{PS}(Q_1^2,Q_2^2,Q_3^2) = F_{PS^*\gamma^*\gamma^*}\left(Q_2^2;Q_2^2,0\right)\times \\ \times F_{PS^*\gamma^*\gamma^*}\left(Q_2^2;Q_1^2,Q_3^2\right)\mathrm{Tps}_{\mathbf{1,2}}, \\ \mathcal{N}_{1,2}^{S}(Q_1^2,Q_2^2,Q_3^2) = A_{S^*\gamma^*\gamma^*}\left(Q_2^2;Q_2^2,0\right)\times \\ \times\left[A_{S^*\gamma^*\gamma^*}\left(Q_2^2;Q_1^2,Q_3^2\right)\mathrm{Ts}_{\mathbf{1,2}}^{AA}+\right. \\ \left.+\frac{1}{2}\mathrm{B}_{S^*\gamma^*\gamma^*}\left(Q_2^2;Q_1^2,Q_3^2\right)\mathrm{Ts}_{\mathbf{1,2}}^{\mathrm{AB}}\right], \tag{42}$$

where $Q_3 = -(Q_1+Q_2)$, $t = (Q_1Q_2)/(|Q_1|\,|Q_2|)$. The universal kinematic factors $\mathrm{Tps}_{\mathbf{1,2}}$ and $\mathrm{Ts}_{\mathbf{1,2}}$ obtained after averaging over the directions of muon momentum p can be found in [1] and [39], correspondingly. We would like to stress that the integral representation (42) is valid for any vertices F, A, B.

For numerical estimations in the NχQM we use the Gaussian nonlocal form factor

$$f\left(k^2\right) = \exp\left(-k^2/2\Lambda^2\right). \tag{43}$$

As to the model parameters, the dynamical quark mass m_d is taken in the typical interval 200–350 MeV and then other parameters (the current quark masses m_c and the nonlocality parameter Λ) are fitted by the pion mass and the two-photon decay constant in correspondence with the pion lifetime given within the error range of PDG in [56]. The results are given in Table 1. Within the NχQM, we found that the pseudoscalar meson contributions to a_μ are systematically lower then the results obtained in the other works. The full kinematic dependence of the vertices on the pion virtuality[7)] diminishes the result by about 20–30 % as compared to the case where this dependence is neglected. For η and η' mesons the results are reduced by factor about 3 in comparison with the results obtained in other models where the kinematic dependence was neglected (see Fig. 2). The scalar mesons contribution is small and partially compensates model dependence of the pseudoscalar contribution (Fig. 8).

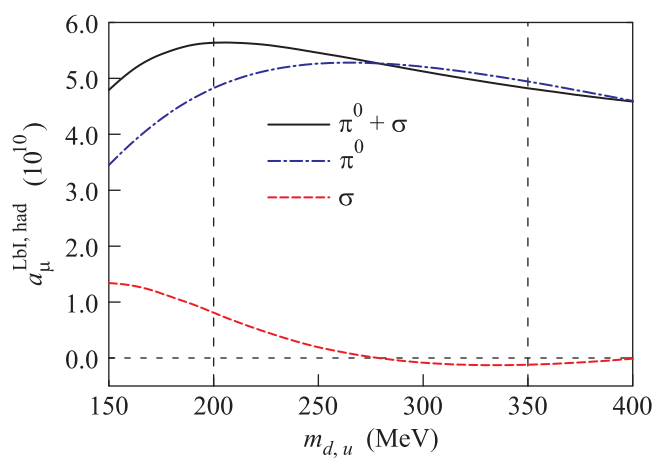

Fig. 8. The HLbL contribution to a_μ from the neutral pion and σ exchanges as a function of the dynamical quark mass. The lower line correspond to the σ contribution, the π^0 contribution is in the middle, and the upper line is the combined contribution. Vertical thin dashed lines denote the interval of dynamical quark masses used for the estimation of the error band for a_μ^{LbL}

7) Later, this dependence was also studied in [41].

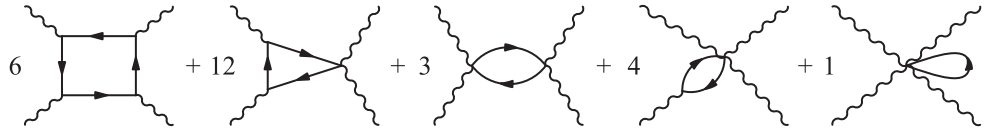

Fig. 9. Contact terms which are gave contribution to $\Pi_{\mu\nu\lambda\rho}(q_1, q_2, q_3)$. Numbers in front of diagrams are the degeneracy factors

The NχQM estimate for the contribution of the dynamical quark box to a_μ[8)], including the contact terms (see Fig. 9), is given in Table 1. One can see that the momentum dependent dynamical mass leads to increasing of contribution of diagram with pure local quark–anti-quark–photon vertices in comparison with constant quark mass. This behavior can be expected since $m(k^2 \to \infty) \to m_c$. The specific feature of these calculations is that there is strong compensation between the contributions from the box diagram with dynamical quarks and local vertices γ^μ, the box diagrams with at least one nonlocal vertex $\Delta\Gamma_\mu^{(1)}(q)$ and all other types of nonlocal diagrams with contact vertices.

6. Conclusions. We briefly discussed the current status of experimental and theoretical results on the electron and muon AMM, $g-2$. These quantities, measured and calculated with very high accuracy, provide a very hard test of the SM. In particular, the electron AMM tests QED at very short distances and now provides the best determination of the fine structure constant α. The muon AMM is much more sensitive to the effects of physics beyond the SM. Presently, there is mismatch between the latest experimental BNL measurements and SM calculations at the level of 3–4 σ. It is the largest deviation in elementary particle physics from the SM predictions. It may be evidence for the existence of new interactions and stringently constraints the parametric space of hypothetical interactions extending the SM. Nowdays, the interest in this problem became lively again in view of the preparation of new Fermilab and J-PARC experiments planning to achieve a measurement precision at the 0.14 ppm level. On the other hand, the biggest theoretical uncertainty is due to the hadronic part of $a_\mu^{\rm SM}$, especially from HVP and HLbL. In this work we considered the latest achievements in phenomenological and model approaches to estimates of leading and next-to-leading order hadronic corrections to $a_\mu^{\rm SM}$. Further studies are needed in order to get better control over the hadronic corrections and reach a precision of calculations comparable to or better than the experimental one.

[8)] Details of calculations of the box diagram in NχQM will be presented elsewhere [45].

We thank Yu.M. Bystritskiy, A.L. Kataev, N.I. Kochelev, E.A. Kuraev, V.P. Lomov, A. Nyffeler, H.-P. Pavel, A.A. Pivovarov for critical remarks and illuminating discussions. This work is supported in part by the Russian Foundation for Basic Research (projects # 11-02-00112 and 12-02-31874).

Numerical calculations have been carried out on the Matrosov computing cluster of ISDCT.

1. F. Jegerlehner and A. Nyffeler, Phys. Rep. **477**, 1 (2009).
2. J. P. Miller, E. de Rafael, B. L. Roberts, and D. Stuckinger, Ann. Rev. Nucl. Part. Sci. **62**, 237 (2012).
3. D. Hanneke, S. Fogwell, and G. Gabrielse, Phys. Rev. Lett. **100**, 120801 (2008).
4. T. Aoyama, M. Hayakawa, T. Kinoshita, and M. Nio, Phys. Rev. Lett. **109**, 111807 (2012).
5. T. Kinoshita, Int. J. Mod. Phys. A **29**, 1430003 (2014).
6. S. Laporta and E. Remiddi, Phys. Lett. B **379**, 283 (1996).
7. P. J. Mohr, B. N. Taylor, and D. B. Newell, Rev. Mod. Phys. **84**, 1527 (2012).
8. R. Bouchendira, P. Clade, S. Guellati-Khelifa, F. Nez, and F. Biraben, Phys. Rev. Lett. **106**, 080801 (2011).
9. G. W. Bennett et al. (Muon (g–2) Collaboration), Phys. Rev. D **73**, 072003 (2006).
10. G. Venanzoni (Fermilab E989 Collaboration), J. Phys. Conf. Ser. **349**, 012008 (2012); http://gm2.fnal.gov/.
11. N. Saito (J-PARC g–2/EDM Collaboration), AIP Conf. Proc. **1467**, 45 (2012).
12. T. Aoyama, M. Hayakawa, T. Kinoshita, and M. Nio, Phys. Rev. Lett. **109**, 111808 (2012).
13. A. Czarnecki, W. J. Marciano, and A. Vainshtein, Phys. Rev. D **67**, 073006 (2003) [Erratum-ibid. D **73** , 119901 (2006)].
14. C. Gnendiger, D. Stockinger, and H.Stockinger-Kim, Phys. Rev. D **88**, 053005 (2013).
15. G. Aad et al. (ATLAS Collaboration), Phys. Lett. B **716**, 1 (2012).
16. G. Aad et al. (ATLAS Collaboration), Phys. Lett. B **726**, 88 (2013).
17. S. Chatrchyan et al. (CMS Collaboration), Phys. Lett. B **716**, 30 (2012).
18. S. Chatrchyan et al. (CMS Collaboration), Phys. Rev. Lett. **110**, 081803 (2013).

19. C. Bouchiat and L. Michel, J. Phys. Radium **22**, 121 (1961); L. Durand, Phys. Rev. **128**, 441 (1962); M. Gourdin and E. De Rafael, Nucl. Phys. B **10**, 667 (1969).
20. M. Davier, A. Hoecker, B. Malaescu, and Z. Zhang, Eur. Phys. J. C **71**, 1515 (2011) [Erratum-ibid. C **72**, 1874 (2012)].
21. K. Hagiwara, R. Liao, A. D. Martin, D. Nomura, and T. Teubner, J. Phys. G **38**, 085003 (2011).
22. F. Jegerlehner and R. Szafron, Eur. Phys. J. C **71**, 1632 (2011).
23. J. Prades, E. de Rafael, and A. Vainshtein, in *Advanced Series on Directions in High Energy Physics*, v. 20; arXiv:0901.0306 [hep-ph].
24. S. Laporta and E. Remiddi, Phys. Lett. B **301**, 440 (1993).
25. J. H. Kuhn, A. I. Onishchenko, A. A. Pivovarov, and O. L. Veretin, Phys. Rev. D **68**, 033018 (2003).
26. E. de Rafael, Phys. Lett. B **322**, 239 (1994).
27. M. Hayakawa, T. Kinoshita, and A. I. Sanda, Phys. Rev. Lett. **75**, 790 (1995); M. Hayakawa and T. Kinoshita, Phys. Rev. D **57**, 465 (1998) [Erratum-ibid. D **66**, 019902 (2002)].
28. J. Bijnens, E. Pallante, and J. Prades, Phys. Rev. Lett. **75**, 1447 (1995); J. Bijnens, E. Pallante, and J. Prades, Nucl. Phys. B **474**, 379 (1996); B **626**, 410 (2002).
29. M. Knecht and A. Nyffeler, Phys. Rev. D **65**, 073034 (2002).
30. K. Melnikov and A. Vainshtein, Phys. Rev. D **70**, 113006 (2004).
31. A. Nyffeler, Phys. Rev. D **79**, 073012 (2009).
32. K. Kampf and J. Novotny, Phys. Rev. D **84**, 014036 (2011).
33. P. Roig, A. Guevara, and G. L. Castro, Phys. Rev. D **89**, 073016 (2014).
34. E. Bartos, A. Z. Dubnickova, S. Dubnicka, E. A. Kuraev, and E. Zemlyanaya, Nucl. Phys. B **632**, 330 (2002).
35. A. A. Pivovarov, Phys. Atom. Nucl. **66**, 902 (2003) [Yad. Fiz. **66**, 934 (2003)]; hep-ph/0110248.
36. J. Erler and G. T. Sanchez, Phys. Rev. Lett. **97**, 161801 (2006).
37. R. Boughezal and K. Melnikov, Phys. Lett. B **704**, 193 (2011).
38. D. Greynat and E. de Rafael, JHEP **1207**, 020 (2012).
39. A. E. Dorokhov and W. Broniowski, Phys. Rev. D **78**, 073011 (2008); A. E. Dorokhov, A. E. Radzhabov, and A. S. Zhevlakov, Eur. Phys. J. C **71**, 1702 (2011).
40. A. E. Dorokhov, A. E. Radzhabov, and A. S. Zhevlakov, Eur. Phys. J. C **72**, 2227 (2012).
41. T. Goecke, C. S. Fischer, and R. Williams, Phys. Rev. D **83**, 094006 (2011) [Erratum-ibid. D **86**, 099901 (2012)]; Phys. Rev. D **87**, 034013 (2013).
42. D. K. Hong and D. Kim, Phys. Lett. B **680**, 480 (2009).
43. L. Cappiello, O. Cata, and G. D'Ambrosio, Phys. Rev. D **83**, 093006 (2011).
44. T. Blum, A. Denig, I. Logashenko, E. de Rafael, B. L. Roberts, T. Teubner, and G. Venanzoni, hep-ph/1311.2198.
45. A. E. Dorokhov, A. E. Radzhabov, and A. S. Zhevlakov, in preparation.
46. E. Pallante, Phys. Lett. B **341**, 221 (1994); B. Holdom, R. Lewis, and R.R. Mendel, Z. Phys. C **63**, 71 (1994); T. Goecke, C. S. Fischer, and R. Williams, Phys. Lett. B **704**, 211 (2011).
47. A. E. Dorokhov, Phys. Rev. D **70**, 094011 (2004).
48. A. L. Kataev, Phys. Rev. D **86**, 013010 (2012).
49. A. Kurz, T. Liu, P. Marquard, and M. Steinhauser, Nucl. Phys. B **879**, 1 (2014).
50. I. V. Anikin, A. E. Dorokhov, and L. Tomio, Phys. Part. Nucl. **31**, 509 (2000) [Fiz. Elem. Chast. Atom. Yadra **31**, 1023 (2000)].
51. A. E. Dorokhov and W. Broniowski, Eur. Phys. J. C **32**, 79 (2003).
52. A. E. Dorokhov, Eur. Phys. J. C **42**, 309 (2005); A. E. Dorokhov, JETP Lett. **82**, 1 (2005) [Pisma v ZhETF **82**, 3 (2005)].
53. A. E. Dorokhov, Acta Phys. Polon. B **36**, 3751 (2005).
54. S. Mandelstam, Annals Phys. **19**, 1 (1962); J. Terning, Phys. Rev. D **44**, 887 (1991).
55. S. J. Brodsky and E. De Rafael, Phys. Rev. **168**, 1620 (1968).
56. J. Beringer et al. (Particle Data Group Collaboration), Phys. Rev. D **86**, 010001 (2012).